Monitoring Two-Dimensional Coordination Reactions: Directed Assembly of Co−Terephthalate Nanosystems on Au(111)

Sylvain Clair,*,†,⊥ Stéphane Pons,†,# Stefano Fabris,‡ Stefano Baroni,‡ Harald Brune,† Klaus Kern,†,§ and Johannes V. Barth*,†,∥

Institut de Physique des Nanostructures, Ecole Polytechnique Fédérale de Lausanne, CH-1015 Lausanne, Switzerland, INFM-CNR DEMOCRITOS National Simulation Center and SISSA, Via Beirut 2-4, I-34014 Trieste, Italy, Max-Planck-Institut für Festkörperforschung, Heisenbergstrasse 1, D-70569 Stuttgart, Germany, and Departments of Chemistry and Physics & Astronomy, University of British Columbia, Vancouver, BC V6T 1Z4, Canada

Received: December 12, 2005; In Final Form: January 21, 2006

We report scanning tunneling microscopy observations on the formation of 2D Co-based coordination compounds on the reconstructed Au(111) surface. Preorganized arrays of Co bilayer islands are shown to be local reaction sites, which are consumed in the formation of Co−terephthalate aggregates and regular nanoporous grids. The latter exhibit a planar geometry stabilized by the smooth substrate. The nanogrids are based on a rectangular motif, which is understood as an intrinsic feature of a 2D cobaltous terephthalate sheet and dominates over the templating influence of the quasihexagonal substrate atomic lattice. The dynamics of the Co island dissolution and metallosupramolecular self-assembly could be monitored in situ. Complementary first-principles calculations were performed to analyze the underlying driving forces and to examine general trends in 2D metal−carboxylate formation. The findings indicate the wide applicability of coordination chemistry concepts at surfaces, which moreover can be spatially confined by using templated substrates, and its potential to synthesize arrangements unavailable in bulk materials.

1. Introduction

The metal-directed assembly of organic linker molecules provides versatile strategies for the synthesis of supramolecular architectures[1−3] and novel nanoporous materials.[4−6] Recent findings revealed that similar design principles can be employed to fabricate nanoscale metal−organic systems on surfaces.[7,8] In particular, a series of low-dimensional Fe−carboxylate nanostructures were obtained under ultrahigh vacuum (UHV) conditions, including mononuclear arrays, nanoporous 2D metal−organic coordination networks, as well as ladder structures and metal−organic coordination chains.[7,9−13] So far, these systems have been mostly realized on homogeneous substrates where organic precursor layers were employed to react with small doses of evaporated Fe atoms representing transition-metal centers. Recently, we demonstrated that metallosupramolecular texturing of a surface is possible by using an inhomogeneous Au(111) substrate patterned with iron dots to steer a surface complexation reaction.[25] Here, we report the first investigation on Co-based coordination compounds at a metal surface exploiting a similar approach. The weak chemical reactivity of gold and the low surface corrugation of the densely packed (111) orientation provide an inert substrate, on which the intrinsic mechanisms of Co complexation reactions at surfaces are expressed. The substrate reconstruction offers the possibility to grow natural nanoscopic Co-island arrays, which allow one to spatially localize the reaction. Our scanning tunneling microscopy (STM) observations provide exquisite insight into the mechanism of the complexation readily occurring with co-deposited terephthalate linkers. First-principles calculations provide a complementary understanding of the experimental results and insert them into a wider perspective that also helps to rationalize previous findings. This analysis reveals general trends on the energetics for 2D metal−carboxylate formation and indicates the wide applicability of the developed concepts in surface coordination chemistry.

2. Experimental and Theoretical Section

All experiments were performed with a home-built ultrahigh vacuum scanning tunneling microscope (UHV-STM).[14] The system base pressure was below 3×10^{-10} mbar. The Au(111) surface was prepared by repeated cycles of argon sputtering (900 eV, 5 μA/cm^2) followed by annealing at 900 K. The terephthalic acid (1,4-benzenecarboxylic acid, abbreviated TPA) molecules (Fluka, >99%) were first outgassed in a vacuum for several hours and then evaporated from a Knudsen cell at 150 °C onto the substrate kept at room temperature. This provided a deposition rate of about one monolayer (ML) per minute. Co atoms were evaporated using an electron-beam heating evaporator. The STM head is of the Besocke type and runs with commercial control electronics (RHK - SPM100). The STM tip is made out of an etched W wire (Ø 0.7 mm) and was prepared by Ar-bombardment in UHV. All data presented here were acquired at room temperature in the constant current mode, with typical tunneling resistances in the range of 10−1000 MΩ.

* Corresponding authors. E-mail: sclair@riken.jp (S.C.); jvb@chem.ubc.ca (J.V.B.).
† Ecole Polytechnique Fédérale de Lausanne.
‡ INFM-CNR DEMOCRITOS National Simulation Center and SISSA.
§ Max-Planck-Institut für Festkörperforschung.
∥ University of British Columbia.
⊥ Present address: RIKEN, The Institute for Physical and Chemical Research, 2-1 Hirosawa, Wako, Saitama 351-0198, Japan.
Present address: Laboratoire de Physique des Matériaux, Université Henri Poincaré, Nancy I - Boîte Postale 239, F-54506 Vandoeuvre-lès-Nancy, France.

10.1021/jp057239s CCC: $33.50
Published on Web 02/25/2006

In the figure captions, *V* refers to the bias applied to the sample. For TPA, 1 ML refers to a complete layer of the densely packed hydrogen-bonded phase described elsewhere,[15] corresponding to a ~1:9 ratio between adsorbed molecules and substrate atoms. For Co, 1 ML refers to an idealized commensurate monatomic film on Au(111), that is, with one cobalt per substrate atom.

The ab initio calculations were based on density functional theory (DFT), with the exchange and correlation energy functional expressed in the Perdew−Burke−Ernzerhof generalized gradient approximation.[16] The plane-wave pseudo-potential method was used to solve the resulting Kohn−Sham equations, as implemented in the PWscf/quantum-ESPRESSO computer package.[17] Ions were represented by ultrasoft pseudopotentials,[18] and the kinetic cutoffs limiting the wave function basis set and the charge density Fourier expansion were 408.18 and 4081.80 eV, respectively. Metal−organic complexes and TPA molecules in the gas phase were modeled with orthorhombic supercells of dimensions 1.589 nm (in the plane of the TPA aromatic ring) and 0.794 nm (out of that plane). The calculations were performed at the Γ point. The Au(111) surface (clean and with adsorbed metal adatoms) was simulated with (2×2) supercell slabs, 6 atomic-layers thick. The two opposing surfaces were separated by 1.544 nm of vacuum. The Brillouin-zone sampling was performed with a (6×6×1) *k*-point mesh generated with the method of Monckhorst−Pack[19] and with a Methfessel−Paxton smearing[20] of 0.07 eV. The energy for the isolated transition-metal atoms was calculated in cubic supercells (a = 1.058 nm). Note that this is just a reference energy. It is used only to define the energy contributions Δ^{gas} and Δ^{surf} as described below. The metal bulk cohesion energies Δ^{coh} were taken from experiment.[21]

3. Results and Discussion

STM Observations. The (22×√3) reconstruction of the Au(111) surface implies a local 4% uniaxial contraction of the surface layer in a ⟨1$\bar{1}$0⟩ direction. The contraction direction periodically alternates by 120°, which accounts for mesoscopic reconstruction domains resolved by STM as chevron pattern.[22] This superstructure is suitable to steer the growth of transition-metal nanoarrays, because the dislocations at the turns in the reconstruction lines (the elbows) provide preferential nucleation sites.[23] Thus, cobalt adatoms condense in regularly distributed bilayer islands at room temperature.[24] The corresponding ideal superlattice unit cell is close to rectangular and ~7 × 15 nm^2 in size (cf., Figure 1a; note that substantial variations can occur on small terraces and in the vicinity of defects). A deposition of 0.1 ML produces islands comprising on average ~150 Co atoms.

In Figure 1b, we present an STM image showing the situation upon exposing a 0.08 ML Co nanoarray to a dose of 0.3 ML TPA on Au(111) at room temperature. Each Co cluster contained initially ~120 atoms. Two distinct phases are observed. The minority phase in the lower part of the image (A) comprises extended close-packed organic domains, which are readily identified as pure organic layers, in agreement with our previous STM study dealing exclusively with TPA self-assembly on Au(111).[15] Here, the intermolecular cohesion is mediated by hydrogen bonding, with some Co islands being simply trapped in the organic sheet. By contrast, in the upper part of the image (B), the majority phase identified by a markedly different open network structure is emerging. Here, the size of the Co islands is reduced, providing evidence for their partial dissolution and the formation of metal−organic compounds. This interpretation is similarly supported by the ramified shape of the islands that

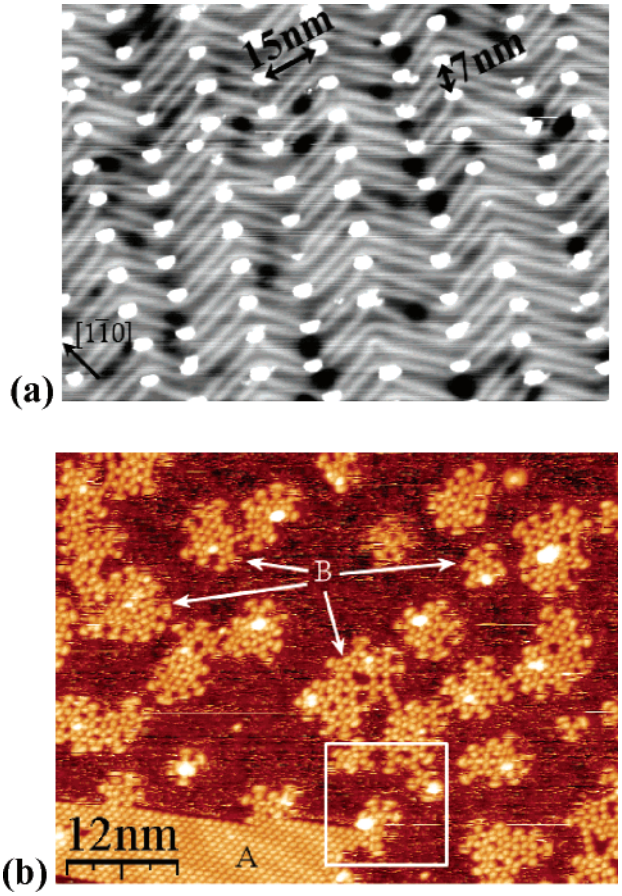

Figure 1. (a) Array of cobalt clusters following evaporation of 0.14 ML Co on the Au(111) surface at room temperature. The deposited atoms condense in bilayer islands at the elbow sites of the chevron reconstruction. The Co dots contain on the average ~200 atoms representing in situ nano-reservoirs for the formation of metal−organic complexes with co-deposited carboxylic acids (STM image size 100 × 80 nm^2, I = 1.3 nA, V = 20 mV). (b) Complexation reaction following deposition of 0.3 ML TPA on a Co array (0.08 ML, corresponding to ~120 atoms per island) on Au(111) at room temperature. A minority of hydrogen-bonded domains (A) coexists with the dominating metal−organic compounds (B) evolving around residual Co dots (I = 0.6 nA, V = −0.7 V).

cannot be stabilized by hydrogen bonding. The complexes decorate the residual Co dots and form irregular 2D clusters, whereby some Co islands were even completely dissolved. The noisy background between is accordingly associated with a 2D gas phase of highly mobile adspecies, which may stick to the border of these clusters or be released by formation or dissociation of lateral linkages.

Hence, there are two competing and parallel processes. On one hand, the integral TPA molecules tend to organize in a dense phase through dimerization of their carboxyl groups.[15] Within a domain, the close packing and intermolecular cohesion prevent any mobility. The domain cohesion is possibly further increased by the Co clusters trapped inside the domains, which act as anchoring pillars and restrain molecular rearrangements. The hydrogen bonding induces appreciable stability of the domain boundaries, therefore preventing the incorporation of metals. The high TPA sheet cohesion is demonstrated furthermore by its stability against annealing up to a temperature of 330 K. On the other hand, the majority of the molecules react with the Co atoms to form terephthalate species, which is inferred from the ramified shape of the respective islands and the pertaining cobalt island dissolution. This reaction is irreversible due to the

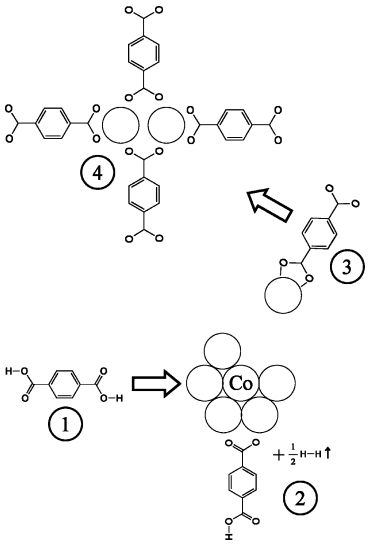

Figure 2. Schematics of the Co−terephthalate complexation reaction. (1) Transport of the molecule to the Co cluster. (2) Deprotonation of the carboxyl group and thermal desorption of molecular hydrogen. (3) Diffusion of Co−terephthalate species to form Co−TPA nanogrid elements (4). Metal−metal and intermolecular bonding distances are to scale.

deprotonation of the carboxylic groups and the subsequent surface desorption of molecular hydrogen (cf., discussion below). The equilibrium state between these two competing processes is determined by the stability of the hydrogen-bonded domains, which is related to the total density of the molecular species deposited on the surface, to the relative stoichiometry metal/molecules, and to a kinetic factor determined by the deposition rate and the surface mobility (controlled by the substrate temperature during deposition; note that a reversal of the deposition sequence thus strongly changes the reaction scenario). By a fine-tuning of these parameters, we could steer the formation of distinct metallosupramolecular nano-architectures.[25]

The formation of coordination structures requires the deprotonation of the molecular carboxyl groups. That is, in the presence of Co, TPA readily reacts to form diterephthalate, which is engaged in the formation of metal−ligand bonds. The pertaining chemical reaction can be formally represented by the following net equation (see also the schematized reaction scenario in Figure 2):

$$2\mathrm{R{-}(COOH)} + \mathrm{Co}_n \rightarrow \mathrm{Co}_n(\mathrm{R{-}COO})_2 + \mathrm{H}_2\uparrow \qquad (1)$$

Adsorbed atomic hydrogen appears as an intermediate reaction product, which readily recombines into molecular hydrogen and desorbs.[26] Reaction 1 represents therefore a one-way path. From the formal point of view of electron transfer, the desorbed hydrogen molecule takes over the electrical charge, which is necessary for the oxidation of the metal center. The mechanism described here provides a simple and general picture, which does not take into account explicitly the influence of the substrate. The latter acts as an anchoring surface with a periodic potential that influences the relative geometry of the reactants, as well as an electron source, which can screen the electrical charges[27] held by the adsorbates. The indirect participation of the substrate in the chemical reaction is therefore an important factor.

The kinetics of the formation of metal−ligand bonds correlates with a time constant of the order of 1 min at room temperature for typical deposition parameters such as those employed in Figure 1b. The shape of the clusters is thus changing from frame to frame during sequential imaging with STM. In particular, Figure 3 shows the temporal evolution of a representative cluster. An inspection of frames #2 and 3 (recorded 7 and 14 min after frame #1, respectively) reveals that the size of the metal core has decreased and more metal−organic complexes are connected to it. However, in frame #4 (after 21 min), the size of the aggregate has shrunk again, indicating that dissociation and exchange of metal−organic species with the 2D gas phase occurred (see Supporting Information for a full sequence of STM images).

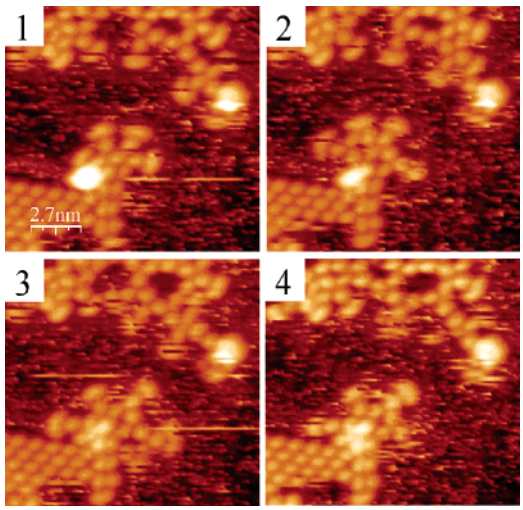

Figure 3. In situ monitoring of Co island dissolution. The temporal evolution of the area marked by the white frame in Figure 1b reveals that some of the cobalt atoms from the core of the cluster are consumed in the formation of the connected complexes (frames #2, 3), which subsequently partly dissociate (frame #4; time lapse between images 0, 7, 14, and 21 min, respectively).

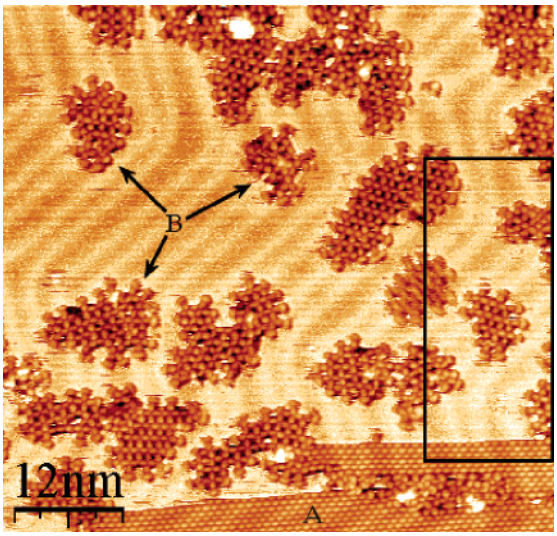

Figure 4. Almost complete dissolution of Co islands and formation of 2D nanoporous metal−organic aggregates upon thermal annealing to 330 K (same reactant concentrations as in Figure 1). Hydrogen-bonded domains (A) comprising partially reacted Co dots coexist with coordination islands showing distinct grid motifs (B) ($I = 0.6$ nA, $V = -0.7$ V).

More regular metal−organic aggregates evolve upon thermal annealing. Figure 4 shows the coordination networks after heating the sample for 20 min at 330 K. Domains of hydrogen-bonded TPA are still present with Co dots trapped in it (lower part); however, at the border of the residual islands now the

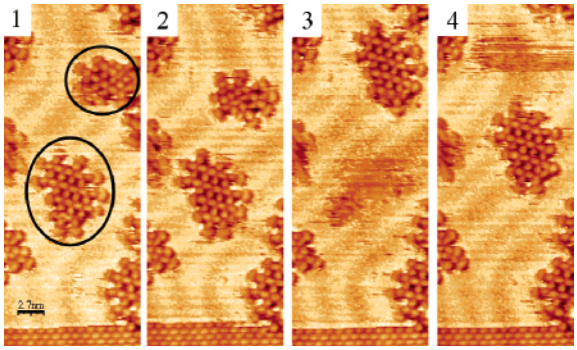

Figure 5. Temporal evolution of the area marked by the black frame in Figure 4 monitoring in situ the shape, internal structure, and motions of metallosupramolecular nanogrids (time lapse between images 0, 8, 15, and 45 min, respectively). While the upper cluster marked in frame 1 dissociates completely, the lower one undergoes marked rearrangements and moves collectively on the surface.

characteristic features of metal−organic complexation are encountered. On the other hand, in the upper part of the image most Co dots have completely disappeared and the metal−organic complexes are well developed organizing in locally regular square or rectangular lattices (nano-grids), surrounded by a 2D gas phase formed by highly mobile Co and TPA species. This implies that locally all of the Co atoms are either involved in Co−carboxylate compounds or present as adatoms. It is therefore thermodynamically favorable to break the strong metallic bond in the islands and to form metal−carboxylate bonds, as corroborated by the DFT calculations discussed in the following. In comparison with the separated reactants, Co in a cluster and di-terephthalate, organizing the compounds in nanogrids lowers the free energy. Moreover, the imaging conditions in this experiment allow one to resolve the distinct pattern of the Au(111) chevron reconstruction, which remains unaffected by the presence of the mixed Co−TPA layer. This demonstrates the moderate substrate coupling of the metal−organic layer and the absence of intermixing or alloy formation between Co and the Au surface. Furthermore, we can monitor in situ metallosupramolecular self-assembly and its dynamics. The nanogrid domains can change their shape and rearrange their internal structure, and even move or dissociate completely. Figure 5 shows a sequence of STM images, illustrating the evolution of two such domains with time (a complete animated sequence of STM images is provided as Supporting Information).

The detailed structure of the nanogrids could not be exactly determined because of the reduced size of the ordered domains and the various possible orientations. The molecular organization is probably closely related to similar grids observed with TPA (or other ditopic carboxylate linkers) and Fe on Cu(100),[11,28] where the coordination center is a di-iron unit that is surrounded by four carboxylate moieties (in contrast to these systems, the metal centers are not directly resolved for the present case). A tentative structural arrangement is shown in the schematic model depicted in Figure 6. However, the reconstructed quasi-hexagonal Au(111) surface is not well suited for the commensurate matching of a rectangular superlattice. The precise structure is therefore subject to the particular symmetry of the substrate modulations and probably not exactly periodic. Further distortions due to the inhomogeneities of the surface reconstruction are expected, similar to the case of pure TPA layers on Au(111), where marked variations in H-bond lengths exist.[15] As a result of this complexity, we observe the coexistence of a variety of different small-sized domains in various orientations

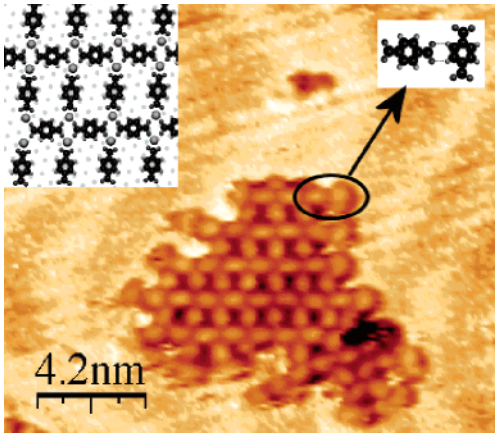

Figure 6. Tentative model for a rectangular metal−organic nanogrid with a Co−TPA stoichiometry of 1:1. The geometry is inspired from the structure of related Fe−TPA coordination networks on the Cu(100) surface.[28] Top-right inset: Characteristic phenyl−carboxylate hydrogen-bonding scheme at the nanogrid rim between two adsorbed diterephthalates reflecting the lack of Co adatoms.

with respect to the substrate. Efforts to improve the ordering by different sample preparations and increased annealing temperatures resulted in the formation of nanogrid domains with an extension of at most a few tens of nanometers. The fact that the coordination compounds do not coherently adapt their structure to the substrate hexagonal symmetry strongly indicates that the shape of the ideal 2D Co−terephthalate compounds is intrinsically a rectangular or square grid. The directional metal−ligand bond is decisive for the precise relative positioning of the reactants, dominating over the influence of the substrate symmetry.

The nanoporous islands show a characteristic decoration at their borders where the open grid motif of the interior is not continued (cf., Figure 6). This phenomenon is attributed to an oversupply of organic linkers, all of which are transformed to terephthalates because of the dynamic nature of the complexation reaction (similarly to carboxylate formation scenarios on Cu substrates[29,30]). The decoration is accordingly understood as follows: the formally negatively charged carboxylate is engaged in hydrogen-bond formation with the phenyl ring of adjacent terephthalate species, thus stabilizing the peculiar perpendicular coupling motif shown in Figure 6. In fact, each molecule involved in a metal−organic bond through only one of its carboxylate groups (i.e., a molecule at the rim of a cluster) forms such a hydrogen bridge with its second carboxylate group. This unusual bonding scheme was also encountered in pure terephthalate/Cu(100) layers.[31] It is made possible by the reduced dimensionality and the presence of a metal substrate and has not been identified in 3D metal−carboxylate compounds.

As compared to 3D bulk crystals, novel geometries are obtained at surfaces because of the 2D confinement upon adsorption where the compounds are influenced by the chemical nature and symmetry of the substrate atomic lattice. For comparison, in the 3D cobaltous terephthalate crystals described in ref 32, the Co atoms occupy octahedral symmetry sites. Such geometry is not directly adaptable on a surface, where different structures with reduced coordination and lower symmetry of the metal centers are favored. The reduced coordination determines a new crystal field geometry, which is associated with coordinatively unsaturated metal centers. This situation is related to the surfaces of oxides, notably investigated for the case of RuO_2, where the chemical reactivity of such sites bestows decisive properties for heterogeneous catalysis.[33,34]

Density Functional Theory Calculations. The formation of 2D surface supported coordination nanosystems depends strongly on the nature of the metal center directing the metallosupramolecular assembly. To rationalize this dependency, we focus on the energetics of a fundamental step in the present carboxylation reaction, that is, the formation of a metal−terephthalate species on Au(111) resulting from a physisorbed TPA molecule and an island of *n* atoms of metal M, expressed as a function of the metal M:

$$(\mathrm{HOOC})-\mathrm{R}-(\mathrm{COOH}) + \mathrm{M}_n \rightarrow \mathrm{M}-\mathrm{OOC}-\mathrm{R}-\mathrm{COO}-\mathrm{M} + M_{n-2} + \mathrm{H}_2 \quad (2)$$

The corresponding driving force Δ[M] is:

$$\Delta[\mathrm{M}] = E^{\mathrm{surf}}[\mathrm{R}-(\mathrm{COO}-\mathrm{M})_2] + E^{\mathrm{gas}}[\mathrm{H}_2] + (n-2)E^{\mathrm{bulk}}[\mathrm{M}] - E^{\mathrm{surf}}[\mathrm{R}-(\mathrm{COOH})_2] - nE^{\mathrm{bulk}}[\mathrm{M}] \quad (3)$$

expressed in terms of the total energies of (i) the metal−terephthalate complex chemisorbed on the surface, $E^{\mathrm{surf}}[\mathrm{R}-(\mathrm{COO}-\mathrm{M})_2]$, (ii) the hydrogen molecule in the gas phase, $E^{\mathrm{gas}}[\mathrm{H}_2]$, (iii) the metal atom M in the bulk phase, $E^{\mathrm{bulk}}[\mathrm{M}]$, and (iv) the molecule physisorbed on the metal surface, $E^{\mathrm{surf}}[\mathrm{R}-(\mathrm{COOH})_2]$. To maintain generality, we aim at identifying trends and relative differences in the chemistry of the process displayed by different transition-metal atoms. In this context, the geometric details of molecular adsorption are neglected to first order, because, for the transition metals considered in this study, they are not expected to be strongly modified upon substitution of the metal M in the molecular complex.[13] The bonding $E^{\mathrm{surf}}[\mathrm{R}-(\mathrm{COO}-\mathrm{M})_2]$ between the metal−terephthalate complex and the surface can be decomposed in the metal−surface and molecule−surface components. The latter is determined by the molecular charge state and by the aromatic π system and is assumed to be mostly independent of the transition-metal species bound to the carboxylate. Apart from a constant shift, the molecule−surface interaction represents in this approximation a minor contribution to the relative surface bonding $E^{\mathrm{surf}}[\mathrm{R}-(\mathrm{COO}-\mathrm{M})_2]$, which in turn is governed by the metal−surface and metal−terephthalate interactions. Hence, Δ(M) can be simplified to:

$$\Delta[\mathrm{M}] = \{E^{\mathrm{gas}}[\mathrm{R}-(\mathrm{COO}-\mathrm{M})_2] + E^{\mathrm{gas}}[\mathrm{H2}] - E^{\mathrm{gas}}[\mathrm{R}-(\mathrm{COOH})_2] - 2E^{\mathrm{gas}}[\mathrm{M}]\} + 2\Delta^{\mathrm{surf}}[\mathrm{M}] - 2\Delta^{\mathrm{coh}}[\mathrm{M}] \quad (4)$$

This expression highlights that the energy Δ is given by three major contributions: The first term in curly brackets is the binding energy in a vacuum of two metal atoms to the carboxylate endgroups. Because this energy involves only species in gas phase, we will refer to it as $\Delta^{\mathrm{gas}}[\mathrm{M}]$. The second term $\Delta^{\mathrm{surf}}[\mathrm{M}]$ is the binding energy of the metal adatom M to the metal surface. The last contribution $\Delta^{\mathrm{coh}}[\mathrm{M}]$ is the cohesion energy of the bulk metal M, that is, the energy gain when incorporating a single atom from the gas phase into a metal island. The difference of the last two energy contributions, $\Delta^{\mathrm{surf}} - \Delta^{\mathrm{coh}}$, approximates the energy required to release from a metal island a surface adatom engaged in complexation.

Expression 4 is used to extract trends and relative differences in the driving force for metal−terephthalate formation induced by transition-metal islands dispersed on Au (111). Here, we analyze the cases of Fe, Co, Ni, Cu, and Au.

For the case of Au, the driving force Δ[Au] is positive, confirming the low reactivity of the Au surface toward metal−organic complex formation, a well-known experimental observation. The presence of Fe, Co, Ni, and Cu on the Au(111) surface increases its reactivity, as shown by the negative formation energies Δ displayed in Figure 7a. Co is the most reactive, followed by Fe. Ni and Cu are the least reactive. The breakdown of the energy Δ in its contributions Δ^{gas}, $2\Delta^{\mathrm{surf}}$, and $2\Delta^{\mathrm{coh}}$ is displayed in Figure 7b−d, respectively. Co atoms form the strongest bond with the carboxylate groups (Figure 7b), while the energy for creating 2 Co adatoms available for metal-carboxylation (2.56 eV) results from the high cohesive energy Δ^{coh} being partially compensated by the strong adhesion Δ^{surf} with the Au(111) surface (Figure 7c and d). Similar energies are necessary to form Fe and Ni adatoms (2.2 and 2.7 eV, respectively), but the corresponding complexation energy is smaller (Figure 7b) than for Co, therefore determining a reduced driving force Δ. The strong reactivity of Co on the Au(111) surface results therefore primarily from the strength of the Co−carboxylate bond. It should be stressed, however, that this factor, represented by $\Delta^{\mathrm{gas}}[\mathrm{M}]$, is not always the dominant contribution. This is clear for the case of Cu: even though it forms the weakest bond with the carboxylic groups (Figure 7b), its low cohesive energy (Figure 7d) makes Cu adatoms easily available on the surface, therefore lowering the overall binding Δ[Cu].

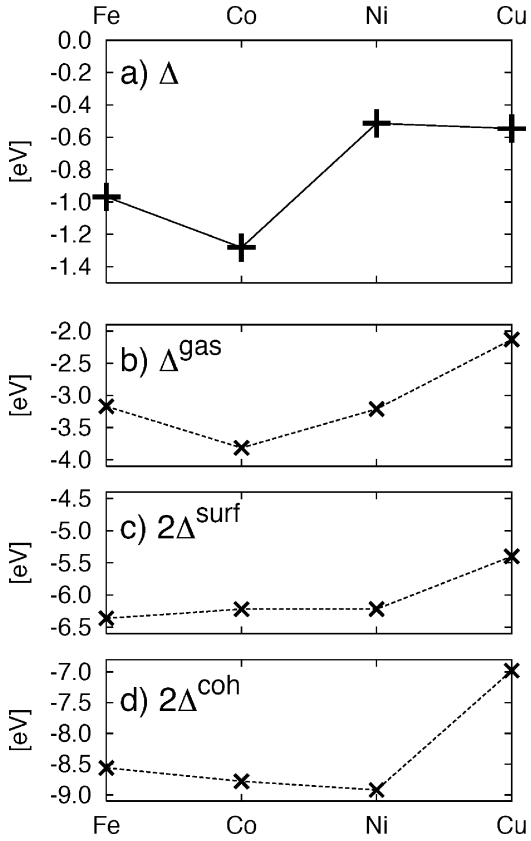

Figure 7. (a) Driving force Δ for metal−carboxylate formation on Au(111) as a function of the transition-metal M, and breakdown in its three contributions as expressed in eq 4: (b) Δ^{gas}, (c) $2\Delta^{\mathrm{surf}}$, and (d) $2\Delta^{\mathrm{coh}}$.

4. Conclusion

In conclusion, we demonstrated the formation of Co−TPA metallosupramolecular nanogrids on the Au(111) surface. The dynamics of the formation−dissociation reaction of these coordination compounds could be monitored directly by sequential STM imaging. The in situ dissolution of the metal clusters in the formation of metal−organic structures upon

annealing was shown. The natural surface patterning of the reconstructed Au(111) could be used successfully to direct the localization of the coordination reaction and the organization of metallosupramolecular nanostructures. Notably, we identified nanoporous grids, which exhibit a planar geometry stabilized by the smooth substrate and comprise a rectangular motif that is understood as an intrinsic feature of a 2D cobaltous terephthalate sheet. The relative energetics controlling their formation were investigated with DFT calculations, which reveal general trends for the metal-carboxylation reaction displayed by different transition metals. The driving forces for metal−terephthalate formation on Au(111) are shown to be determined primarily by the strength of the metal−carboxylate bond, which is maximum for the case of Co.

Acknowledgment. This work was supported by the Swiss National Science Foundation (as part of the European Science Foundation EUROCORES Program SONSs) and the EC Sixth Framework Program (as part of the STREP BioMACH). S.F. acknowledges INFM Progetto Calcolo Parallelo and HPC-EUROPA for computer resources. Images were partly processed with the public domain program WSxM, available at http://www.nanotec.es.

Supporting Information Available: Animated STM image sequences visualizing the dynamics of the complexation reaction (figure 1) and the motion of the metallosupramolecular nanogrids (figure 2). This material is available free of charge via the Internet at http://pubs.acs.org.

References and Notes

(1) Atwood, J. L., Davies, J. E. D., MacNicol, D. D., Vögtle, F., Lehn, J.-M., Eds. *Comprehensive Supramolecular Chemistry*; Pergamon: New York, 1996.

(2) Leininger, S.; Olenyuk, B.; Stang, P. J. *Chem. Rev.* **2000**, *100*, 853−908.

(3) Holliday, B. J.; Mirkin, C. A. *Angew. Chem., Int. Ed.* **2002**, *40*, 2022−2043.

(4) Yaghi, O. M.; O'Keeffe, M.; Ockwing, N. W.; Chae, H. K.; Eddaoudi, M.; Kim, J. *Nature* **2003**, *423*, 705−714.

(5) Kitagawa, S.; Kiraura, R.; Noro, S. *Angew. Chem., Int. Ed.* **2004**, *43*, 2334−2375.

(6) Rao, C. N. R.; Natarajan, S.; Vaidhyanathan, R. *Angew. Chem., Int. Ed.* **2004**, *43*, 1466−1496.

(7) Barth, J. V.; Weckesser, J.; Lin, N.; Dmitriev, S.; Kern, K. *Appl. Phys. A* **2003**, *76*, 645.

(8) Barth, J. V.; Costantini, G.; Kern, K. *Nature* **2005**, *437*, 671.

(9) Dmitriev, A.; Spillmann, H.; Lin, N.; Barth, J. V.; Kern, K. *Angew. Chem., Int. Ed.* **2003**, *41*, 2670−2673.

(10) Spillmann, H.; Dmitriev, A.; Lin, N.; Messina, P.; Barth, J. V.; Kern, K. *J. Am. Chem. Soc.* **2003**, *125*, 10725−10728.

(11) Stepanow, S.; Lingenfelder, M.; Dmitriev, A.; Spillmann, H.; Delvigne, E.; Lin, N.; Deng, X.; Cai, C.; Barth, J. V.; Kern, K. *Nat. Mater.* **2004**, *3*, 229−233.

(12) Dmitriev, A.; Spillmann, H.; Lingenfelder, M.; Lin, N.; Barth, J. V.; Kern, K. *Langmuir* **2004**, *41*, 4799−4801.

(13) Classen, T.; Fratesi, G.; Costantini, G.; Fabris, S.; Stadler, F. L.; Kim, C.; de Gironcoli, S.; Baroni, S.; Kern, K. *Angew. Chem., Int. Ed.* **2005**, *44*, 6142.

(14) Clair, S.; EPF: Lausanne, 2004.

(15) Clair, S.; Pons, S.; Brune, H.; Kern, K.; Barth, J. V. *J. Phys. Chem. B* **2004**, *108*, 14585−14590.

(16) Perdew, J.; Burke, K.; Ernzerhof, M. *Phys. Rev. Lett.* **1996**, *77*, 3865.

(17) Baroni, S.; Dal Corso, A.; de Gironcoli, S.; Giannozzi, P. http://www.pwscf.org.

(18) Vanderbilt, D. *Phys. Rev. B* **1990**, *41*, 7892.

(19) Monckhorst, H. J.; Pack, J. D. *Phys. Rev. B* **1976**, *13*, 5188.

(20) Methfessel, M.; Paxton, A. T. *Phys. Rev. B* **1989**, *40*, 3616.

(21) Lide, D. R., Ed. *CRC Handbook of Chemistry and Physics*; CRC Press: Boca Raton, FL, 1993.

(22) Barth, J. V.; Brune, H.; Ertl, G.; Behm, R. J. *Phys. Rev. B* **1990**, *42*, 9307−9318.

(23) Meyer, J. A.; Baikie, I. D.; Kopatzki, E.; Behm, R. J. *Surf. Sci.* **1996**, *365*, L647.

(24) Voigtländer, B.; Meyer, G.; Amer, N. M. *Phys. Rev. B* **1991**, *44*, 10354.

(25) Clair, S.; Pons, S.; Brune, H.; Kern, K.; Barth, J. V. *Angew. Chem., Int. Ed.* **2005**, *44*, 7294.

(26) Zhou, X.-L.; White, J. M.; Koel, B. E. *Surf. Sci.* **1989**, *218*, 201−210.

(27) Ashcroft, N. W.; Mermin, N. D. *Solid State Phys.* **1976**, 340−342.

(28) Lingenfelder, M. A.; Spillmann, H.; Dmitriev, A.; Stepanov, S.; Lin, N.; Barth, J. V.; Kern, K. *Chem.-Eur. J.* **2004**, *10*, 1913−1919.

(29) Lin, N.; Dmitriev, A.; Weckesser, J.; Barth, J. V.; Kern, K. *Angew. Chem., Int. Ed.* **2002**, *41*, 4779.

(30) Lin, N.; Payer, D.; Dmitriev; Strunskus, A. T.; Wöll, C.; Barth, J. V.; Kern, K. *Angew. Chem., Int. Ed.* **2005**, *44*, 1488.

(31) Stepanow, S.; Strunskus, T.; Lingenfelder, M.; Dmitriev, A.; Spillmann, H.; Lin, N.; Barth, J. V.; Wöll, C.; Kern, K. *J. Phys. Chem. B* **2004**, *108*, 19392−19397.

(32) Kurmoo, M.; Kumagai, H.; Green, M. A.; Lovett, B. W.; Blundell, S. J.; Ardavan, A.; Singleton, J. *J. Solid State Chem.* **2001**, *159*, 343−351.

(33) Over, H.; Kim, Y. D.; Seitsonen, A. P.; Wendt, S.; Lundgren, E.; Schmid, M.; Varga, P.; Morgante, A.; Ertl, G. *Science* **2000**, *287*, 1474.

(34) Wang, J.; Fan, C. Y.; Sun, Q.; Reuter, K.; Jacobi, K.; Scheffler, M.; Ertl, G. *Angew. Chem., Int. Ed.* **2003**, *42*, 2151.